Diamagnetic to paramagnetic transition in $LaCoO_3$

M. J. R. Hoch,[1] S. Nellutla,[1] J. van Tol,[1] Eun Sang Choi,[1] Jun Lu,[1] H. Zheng,[2] and J. F. Mitchell[2]
[1]*National High Magnetic Field Laboratory, Florida State University, Tallahassee, Florida 32310, USA*
[2]*Materials Science Division, Argonne National Laboratory, Argonne, Illinois 60439, USA*
(Received 10 December 2008; revised manuscript received 19 May 2009; published 16 June 2009)

The diamagnetic to paramagnetic spin state transition in $LaCoO_3$ (LCO) that occurs in the temperature range 30–120 K is generally attributed to the small energy gap between the Co^{3+} t_{2g} and e_g states. Evidence for this thermally activated transition has been interpreted as leading to either the intermediate spin state, $t_{2g}^5 e_g^1 (S=1)$, or, alternatively, to the high-spin state, $t_{2g}^4 e_g^2 (S=2)$ of the Co^{3+} ion, with the issue proving highly controversial. In an effort to obtain a consistent description of the temperature dependence of the magnetic and thermal properties of this system, we have made measurements of both the magnetization in applied fields of up to 33 T and the specific heat at 0 and 9 T on a single crystal of LCO. In addition, EPR measurements were made on the same sample using high-field EPR spectrometers. The spin-Hamiltonian parameters are consistent with the previous pulsed-field EPR work and support the atomic-like energy level description of the Co ion. The low-lying first-excited state is part of the $^5T_{2g}$ (^5D) set and is a triplet state with effective spin $S_{\text{eff}}=1$. The magnetization results are analyzed using a mean-field model allowing for antiferromagnetic correlations between the spins. The model is used to estimate the spin contribution to the specific heat.

DOI: 10.1103/PhysRevB.79.214421 PACS number(s): 75.20.Ck, 75.30.Cr, 76.30.−v

I. INTRODUCTION

The Co ion in $LaCoO_3$ (LCO) exists in a diamagnetic low spin (LS) $S=0$ state at low temperatures ($T<20$ K) and in higher spin states for $T>80$ K. The nature of the spin state transition that occurs in the range from 30 to 120 K has been the subject of considerable interest and debate.[1–15] The hybridized electron orbitals that are of importance in determining the magnetic properties of the octahedrally coordinated $3d^6$ Co ion are the t_{2g} and e_g orbitals. The small activation energy of 15 meV between t_{2g} and e_g states in LCO is attributed to competition between the intraionic Hund's rule coupling and the crystal-field splitting. The configuration of the Co^{3+} ion involves six electrons and at low temperatures the LS configuration is $t_{2g}^6 e_g^0$ while at higher temperatures electrons are excited into the e_g levels. It has been suggested that the thermally induced spin state found above 80 K is either the intermediate spin (IS) state, $S=1$ ($t_{2g}^5 e_g^1$), or, alternatively, the high-spin (HS) state $S=2$ ($t_{2g}^4 e_g^2$).

In terms of a single-ion type description the formation of an effective $S=1$ state can be understood using a Hamiltonian that allows for crystal-field (CF) splitting, spin-orbit coupling, and a small zero-field splitting. This form is supported by the electron paramagnetic resonance (EPR) results of Noguchi *et al.*[16] and the theoretical treatment of Ropka and Radwanski.[17] The *d-d* Coulomb interaction results in a ^5D term (25-fold degenerate) which under the effect of the octahedral CF splits into a 15-fold degenerate cubic subterm $^5T_{2g}$ and a 10-fold degenerate ^5E_g subterm at higher energy. The spin-orbit interaction further splits the $^5T_{2g}$ manifold into a triplet, a quintet and a septet with the triplet as the lowest of these levels. If we represent the effective angular momentum by S, then the small trigonal distortion from cubic to rhombohedral symmetry in LCO splits the $S=1$ triplet into a singlet and a doublet separated by D, the zero-field splitting. Furthermore, in this description the low-temperature LS state is the $^1A_1$ state of the Co^{3+} free-ion ^1I term, which becomes the ground state as a result of CF interactions.[17] A representation of the ground state, the low-lying triplet, and quintet states in zero magnetic field are shown in Fig. 1(a). Figure 1(b) shows the ground state and the triplet state ($S=1$) as a function of applied field. It is interesting to note the possibility that triplet-singlet level crossing may be induced by an applied field of ~70 to 80 T dependant on crystal orientation.

Using parameters derived from the EPR results, a theoretical fit to the measured magnetic-susceptibility data has been found to give the correct form but with values that are a factor three too large.[16] An improved fit is obtained using $g=2$.[16] It is possible that changes in the electronic configuration may occur as the population of the e_g states is increased, due to the enhanced hybridization effects with the O $2p$ orbitals leading to a change in g. In this connection it is interesting to note that recent high-temperature EPR spectra obtained at X-band for a series of polycrystalline Sr-doped cobaltites $La_{1-x}Sr_xCoO_3$ (LSCO) ($x=0.1$, 0.2, and 0.3), in which the double exchange and local Jahn-Teller distortions lead to changes in the electronic ground state of the Co ions, give $g\sim 2$.[18] The difference in g values for the undoped and hole-doped crystals has been attributed to the changes in the electronic configuration that lead to the stabilization of an $S=1$ ground state in even lightly doped ($x>1\%$) LSCO, with concomitant changes from atomic-like states to band states but this is not firmly established.[19]

The present work on a single-crystal sample of LCO combines several experimental measurements with a mean-field model in an effort to obtain a consistent description of the spin state transition at temperatures below 200 K. Our studies include continuous-wave (cw) EPR measurements in the frequency range 240–406 GHz at temperatures 4–70 K, magnetization measurements up to 200 K in high magnetic fields and specific-heat measurements in zero field and in 9 T. The EPR measurements in sweepable fields up to 12 T complement the previous pulsed-field work[16] and address, *inter alia*, the question of a possible decrease in g factor with

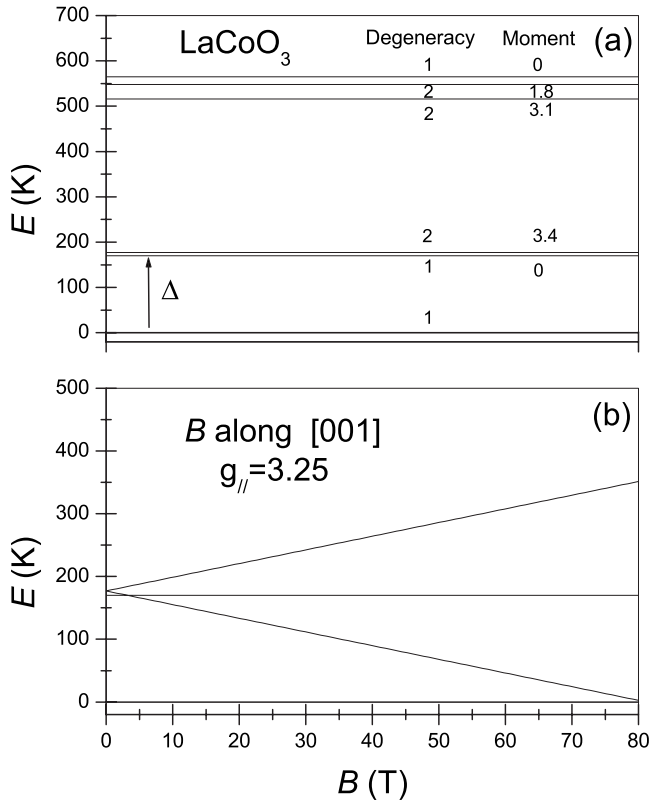

FIG. 1. (a) Co^{3+} ion states for LCO (based on Ref. 17) showing the $^1A_1$ singlet ground subterm, the low-lying triplet arising from the $^5T_{2g}$ subterm of the ^5D term, and some of the higher states, in zero applied field with energies in K. The degeneracies and magnetic moments (in units μ_B) of the various states are indicated. (b) Expanded view of low-lying Co^{3+} ion states for LCO, showing the $^1A_1$ singlet ground subterm and the low-lying triplet from the $^5T_{2g}$ subterm, as a function of applied field B along the pseudocubic [001] direction. The gap Δ and the zero-field splitting D of the $m_S=0$ and the $m_S=\pm 1$ states are discussed in the text. Gap closing is predicted to occur in very high fields. This set of states forms the basis for the model used in analyzing the present experimental results.

temperature. Our other experiments have attempted to detect magnetic field-induced effects, such as departures from linear behavior of the magnetization at fields up to 33 T or changes in the specific heat versus temperature curve. We find that a model based on the EPR results and which explicitly incorporates antiferromagnetic (AFM) spin correlations, satisfactorily accounts for the measured magnetic susceptibility over the temperature range from 4 to 200 K. The model has been used to estimate the magnetic contribution to the specific heat as a function of temperature.

II. EXPERIMENTAL DETAILS

The single-crystal sample of LCO used in the measurements was grown in a floating zone furnace at Argonne National Laboratory and is roughly disk shaped with flat upper and lower surfaces. The pseudocubic [001] trigonal direction (or the [111] direction in the undistorted cubic system) makes an angle of 16° with the normal to the planar surfaces. The EPR spectra provided evidence of twinning in the crystal and this was allowed for in our analysis. Spectra were recorded in the temperature range 20–70 K using either a quasioptical spectrometer, equipped with a goniometer for sample rotation, operating at 240 GHz with a field-swept superconducting magnet (0–12 T) and magnetic field modulation[20] or a variable frequency-transmission spectrometer,[21] with a 17 T sweepable superconducting magnet, at frequencies up to 406 GHz. For the sample rotation measurements a small piece was cut from the sample and mounted on a goniometer device. Above 70 K the linewidths increase significantly preventing measurements at higher temperatures.

Magnetization measurements were made using a vibrating sample magnetometer in the temperature range 1.8–250 K and in applied fields up to 33 T using the high-field facilities at the National High Magnetic Field Laboratory. Specific-heat measurements were made at 0 and 9 T in the temperature range 1.8–200 K using a Quantum Design Physical Property Measurement System (PPMS).

III. RESULTS AND DISCUSSION

Over the temperature range 20–70 K the EPR spectra for the LCO crystal, at all frequencies, correspond to a spin triplet with g values typical of the Co^{3+} ion. Besides the two allowed $\Delta m_s=\pm 1$ transitions, the first-order forbidden tran-

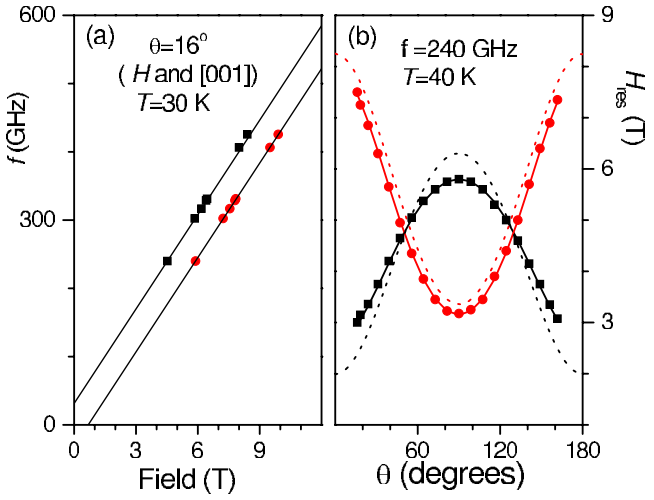

FIG. 2. (Color online) (a) Frequency dependence of $\Delta m_s=\pm 1$ EPR transitions for the single crystal of LCO at 30 K for the magnetic field applied at 16° to the trigonal or pseudocubic [001] axis. Fitted solid lines are based on Eq. (1) with the slopes giving the g value for this orientation while the intercepts are related to the zero-field splitting D. The values obtained are consistent with those given below. (b) Angular dependence of EPR field values for $\Delta m_s=\pm 1$ transitions at 240 GHz and 40 K. Solid lines are fits to Eq. (1) with parameters $g_\parallel=3.25\pm0.01$, $g_\perp=3.83\pm0.01$ and $D=4.5\pm0.3$ cm^{-1}. The dotted lines are simulations of $\Delta m_s=\pm 1$ transitions using spin-Hamiltonian parameters of $g_\parallel=3.35$, $g_\perp=3.55$, and $D=4.9$ cm^{-1} taken from Ref. 16. See text for further details.

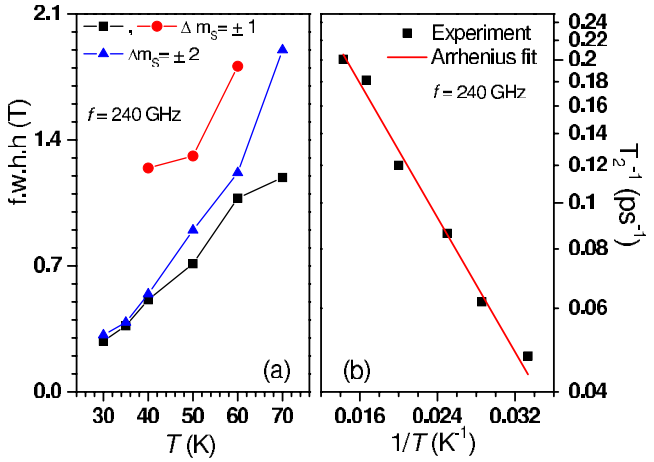

FIG. 3. (Color online) (a) EPR linewidths (f.w.h.h) as a function of temperature for the $\Delta m_s = \pm 1, \pm 2$ transitions obtained at 240 GHz for the applied field perpendicular to the pseudocubic [001] trigonal axis. The linewidths increase with rising T corresponding to a decrease in the spin-spin relaxation time T_2. (b) Temperature dependence of $1/T_2$, calculated from the f.w.h.h of $|0\rangle \rightarrow |1\rangle$ spectra [black squares in Fig. 3(a)]. Solid line is the Arrhenius fit $[1/T_2 = A \exp(-\delta/k_B T)]$ with the parameters $A = 0.7 \pm 0.1$ ps^{-1} and $\delta = 82 \pm 6$ K. See text for details.

sition $\Delta m_s = \pm 2$ is also observed. Narrow spectral components at $g \sim 2$ that persist to 4 K, are attributed to defects and paramagnetic impurities. Figure 2(a) shows a plot of microwave frequency as a function of magnetic field for the $\Delta m_s = \pm 1$ transitions in LCO. The data shown are collected on the transmission spectrometer at 30 K for the field applied 16° to the trigonal axis, i.e., with the sample lower surface perpendicular to the external field H. Figure 2(b) depicts the angular dependence of resonance positions (H_{res}) of $\Delta m_s = \pm 1$ transitions at 40 K and 240 GHz, where 0° corresponds to the applied field parallel to the trigonal axis and 90° corresponds to the applied field perpendicular to the trigonal axis. H_{res} was obtained by fitting the $\Delta m_s = \pm 1$ spectral lines at each orientation using Lorentzian functions.

The rotation patterns shown in Fig. 2(b) were analyzed using the spin Hamiltonian[22]

$$\mathcal{H} = \mu_B \boldsymbol{S} \cdot \tilde{g} \cdot \boldsymbol{H} + D[S_z^2 - S(S+1)/3], \qquad (1)$$

where μ_B is the Bohr magneton, $\boldsymbol{S}$ the spin operator, $\tilde{g}$ the g tensor, and D the zero-field splitting which allows for a small distortion of the unit cell from cubic symmetry. Hyperfine interactions are undetectably small and are omitted in the spin Hamiltonian. The angular dependence can be reproduced very well [see solid lines in Fig. 2(b)] taking $S = 1$ with g-value components $g_{\parallel} = 3.25 \pm 0.01$, $g_{\perp} = 3.83 \pm 0.01$, and zero-field splitting $|D| = 4.50 \pm 0.3$ cm^{-1}. The frequency dependence of the data can also be simulated well [solid line in Fig. 2(a)] with these spin-Hamiltonian parameters. The observed g and D values are in fair agreement with the results of Noguchi *et al.*[16] but with larger g anisotropy ($\Delta g \sim 0.6$) than they found ($\Delta g \sim 0.2$). The dotted lines in Fig. 2(b) give the rotation pattern based on the parameters from Ref. 16.

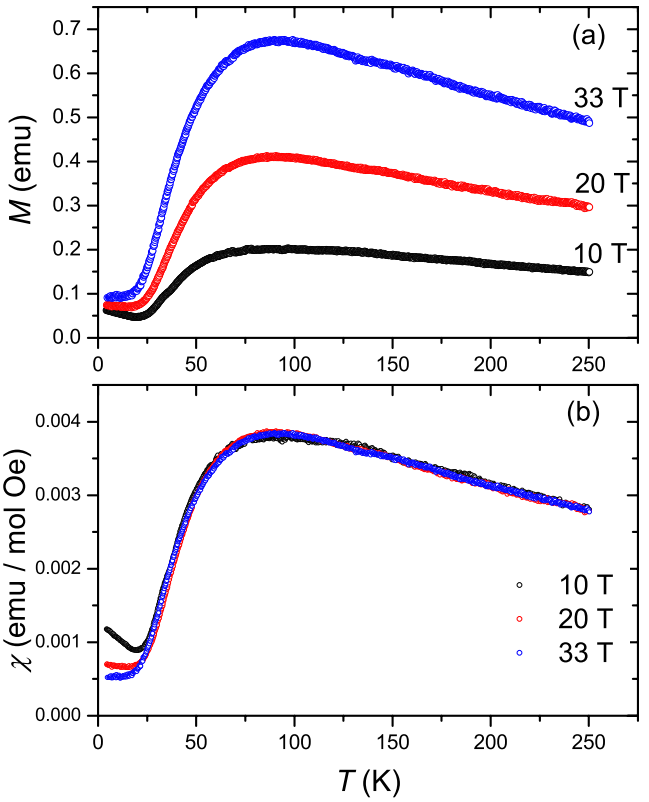

FIG. 4. (Color online) (a) Magnetization curves for the LCO single crystal as a function of temperature in applied fields 10, 20, and 33 T. Measurements were made using a vibrating sample magnetometer. The maximum magnetization at 90 K in 33 T corresponds to 0.227 μ_B/Co. (b) Magnetic susceptibility as a function of temperature obtained from the plots in Fig. 3(a).

The temperature dependence of the EPR spectral linewidths was investigated for a number of fixed crystal orientations at 240 GHz. The three triplet state transitions ($\Delta m_s = \pm 1, \pm 2$) appear only for $T > 25$ K and cannot be detected above 70 K. No evidence for a change in g value with T is found in our temperature dependence studies. The relative intensities of $\Delta m_s = \pm 1$ lines indicate that $D > 0$, in agreement with Noguchi *et al.*[16] The linewidths increase significantly with temperature and the T dependence of the full-width at half-height (FWHH) of the $\Delta m_s = \pm 1, \pm 2$ transitions for H perpendicular to the trigonal direction is plotted in Fig. 3(a). Due to the close proximity of the $|-1\rangle \rightarrow |0\rangle$ transition to $g \sim 2$ impurity spectral features, the linewidth of this component could not be determined reliably at certain temperatures.

As mentioned above, the spectral lines are Lorentzian in shape and the increase in linewidth with T provides evidence for a decrease in the spin-spin relaxation time T_2 linked to lifetime effects. It is likely that a decrease in the spin-lattice relaxation time T_1 occurs in this temperature range through phonon-induced processes and that these processes effectively determine T_2 assuming $T_2 \approx T_1$. Using the relation $T_2 \sim 1/\Delta\omega$, where $\Delta\omega$ is the half-width at half-height in frequency units, T_2 values are obtained and are shown plotted as $1/T_2$ vs $1/T$ in Fig. 3(b). The fitted straight line in Fig. 3(b) corresponds to the energy gap δ in the Arrhenius expres-

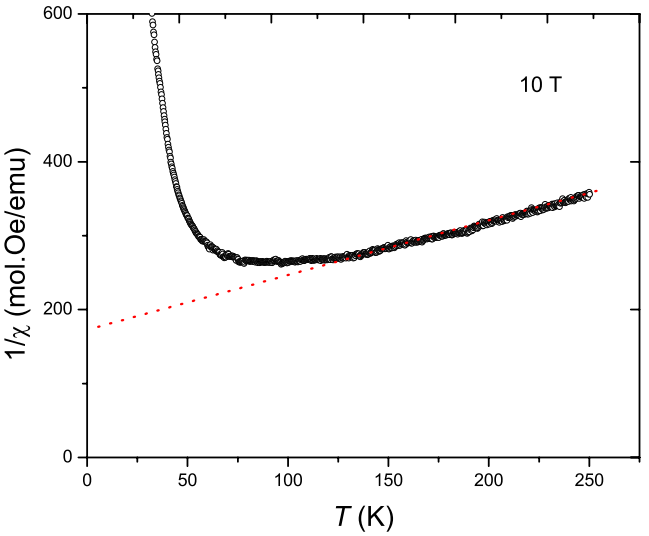

FIG. 5. (Color online) Inverse magnetic susceptibility for LCO versus T. For $T>130$ K the experimental data obey the Curie-Weiss law, shown as the fitted line, with $\theta_{CW}\approx -250$ K. Antiferromagnetic correlations are incorporated in the model that is used in discussing the magnetization and specific-heat results.

sion $1/T_2=A\exp(-\delta/T)$ with $A=0.7\pm0.1$ ps^{-1} and $\delta=82\pm6$ K. δ is about an order of magnitude larger than the Zeeman splitting of the triplet states for $\mu_0 H\sim 5$ T but a factor 2 to 3 times smaller than previous estimates of the singlet-triplet separation Δ shown in Fig. 1. The temperature range covered in Fig. 3(b) is limited by the weakness of the signals below 30 K and the very large linewidths above 60 K. If we assume $1/T_2\sim 1/T_1$ for the $S=1$ triplet levels with phonon-induced transitions, both within the triplet set and between the singlet ground state and the triplet states, responsible for relaxation, then the observed value for δ corresponds to some average of the two energy gaps. It is also

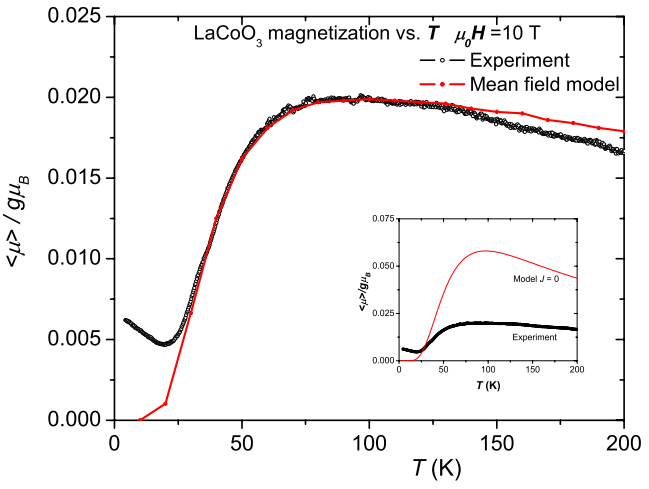

FIG. 6. (Color online) Spin magnetization $\langle\mu\rangle/g\mu_B$ versus T for LCO showing 10 T experimental values from Fig. 4 together with mean-field model predictions based on Eq. (3) in the text. The parameters used in the fit are $\Delta=150$ K, $D=7$ K and $2J=-55$ K. The inset shows a comparison of experimental values with the model assuming *no* AFM correlations ($2J=0$).

possible that AFM correlations, that become increasingly important as T is raised as discussed below, play some role in determining $1/T_2$. The limited range of temperature that is accessible to EPR prevents detailed examination of these possible mechanisms.

The magnetization M as a function of temperature is presented in Fig. 4(a) for the three fields used (10, 20, and 33 T) while Fig. 4(b) shows the magnetic susceptibility χ derived from these results. The maximum M value at 90 K in 33 T corresponds to 0.227 μ_B/Co with μ_B the Bohr magneton. No departure from linear dependence of the magnetization on the applied field is found over the range of fields used except at the lowest temperatures where paramagnetic impurities give rise to the Curie tail that is observed. The χ versus T plot is consistent with previous work.[2,6] A plot of $1/\chi$ versus T is shown as Fig. 5 and reveals Curie-Weiss-type behavior above 130 K with strong departures from this behavior at lower T where the spin state transition becomes important. The temperature intercept at −250 K obtained by

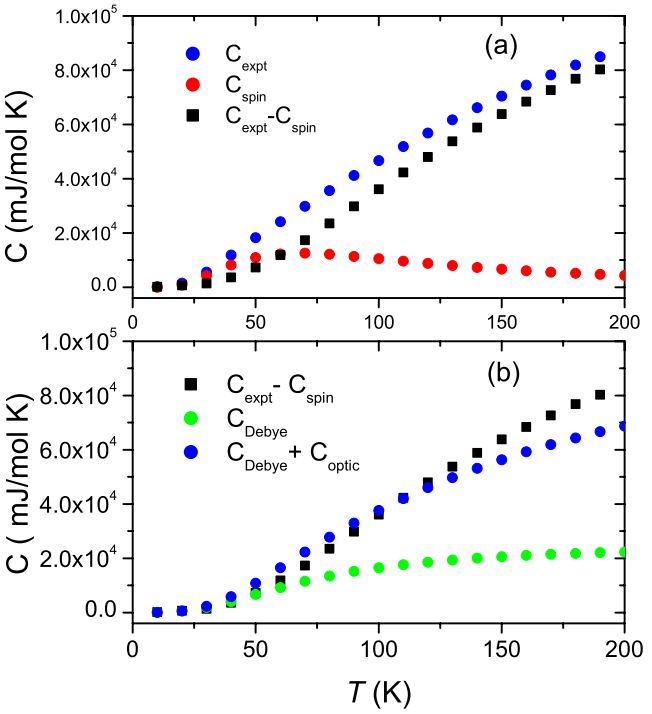

FIG. 7. (Color online) (a) Measured values of the molar specific heat C_{expt} for LCO at 0 T and 9 T as a function of temperature. The PPMS data plots (not shown) for the two applied fields used are indistinguishable. The lower curve designated C_{spin} shows the calculated spin contribution to the specific heat due to the Co^{3+} ion spin state transition obtained using Eq. (4) with $\Delta=150$ K from the magnetization data. (The spin contribution is predicted to be insensitive to fields in the range 0 to 9 T consistent with experiment.) The estimated lattice contribution to the specific heat is obtained by subtracting the calculated magnetic contribution C_{spin} from C_{expt}. (b) Estimated lattice contribution to the specific heat (C_{expt}-C_{spin}) taken from Fig. 7(a) together with the calculated acoustic mode contribution using the Debye model with $\theta_D=300$ K and the acoustic plus three optic phonon modes contribution using the Einstein model for the optic modes with $\theta_E=255$, 453, and 778 K. Further details are given in the text.

extrapolating the Curie-Weiss curve points to the importance of AFM correlations in this undoped system consistent with previous findings in both susceptibility,[2,6] and neutron-scattering experiments.[23] The inelastic neutron-scattering results provide evidence for both ferromagnetic (FM) and AFM dynamical short-range correlations between Co ions in the slightly split (0.6 meV) triplet states. The correlations are temperature dependent and, it is suggested, are linked to orbital order correlations analogous to the *A*-type AFM ordering in $LaMnO_3$.[23] However, instead of static ordering, as found in the manganites, dynamic ordering occurs with correlations in all directions. Glassy behavior in hole-doped $La_{1-x}Sr_xCoO_3$ ($x<0.18$) has been linked to AFM interactions between Co^{3+} ions (designated intermediate spin with $S=1$) in a hole-poor matrix containing FM clusters of double-exchange coupled Co^{3+} and Co^{4+} ions.[24] The nature of the interaction between Co ions in LCO is not well established. The analysis of the present magnetization results suggests that it is the AFM correlations in LCO that play a role in determining this property at the temperatures of interest. Figure 6 shows experimental values of the mean spin magnetization $\langle\mu\rangle/g\mu_B$ from the 10 T data plotted versus T. A theoretical curve based on a mean-field model involving AFM correlations, as described below, provides a good fit to the experimental results. Specific heat C data obtained for the single-crystal sample of LCO in 0 and 9 T is plotted as a function of T in Fig. 7(a). As can be seen an applied field of 9 T produces no measurable change in C.

IV. THEORETICAL MODEL IN MEAN-FIELD APPROXIMATION

Figure 1(b) shows the low lying set of energy levels for Co^{3+} in LCO based on the previous EPR findings,[16] theoretical calculations,[17] and supported by the present EPR results. These levels are important in calculating thermodynamic quantities at temperatures up to 200 K as a function of applied magnetic field. As mentioned in the introduction, the electronic levels of interest for the Co^{3+} ion are those in the first excited $S=1$ triplet state, arising from the $^5T_{2g}$ (^5D) term in the $|LSL_zS_z\rangle$ space, and the ground state $^1A_1$ (^1I) situated at an energy Δ below the triplet state.[17] The trigonal distortion produces a small zero-field splitting D. Other states arising from the 15-fold degenerate $^5T_{2g}$ subterm, some of which are shown in Fig. 1(a), are at sufficiently high energies (>350 K) above the triplet state to make only a small contribution to the partition function at temperatures below 200 K.

Using the energy states shown in Fig. 1(b) and initially ignoring interactions between Co^{3+} ions, the partition function for the magnetic system of N localized spins in applied field H is given by $Z=[1+e^{-\beta\Delta}+e^{-\beta(\Delta+D+g\mu_B\mu_0H)}+e^{-\beta(\Delta+D-g\mu_B\mu_0H)}]^N$ where $\beta=1/k_BT$ with k_B Boltzmann's constant. The magnetization $M=N\langle\mu\rangle$ in terms of the mean magnetic moment per spin $\langle\mu\rangle$, is obtained by differentiation of $\ln Z$ in the usual way. Taking $\beta g\mu_B\mu_0H<1$, which is valid for the temperatures and magnetic fields of interest, gives, to a fair approximation, the magnetic susceptibility as

$$\chi=\frac{2N_Ag^2\mu_B^2\mu_0}{k_BT[2+e^{\Delta/T}+e^{(\Delta+D)/T}]}. \tag{2}$$

AFM interactions have previously been introduced in model calculations for the magnetic susceptibility[6] and we adopt a similar approach. Assuming that only nearest-neighbor interactions need to be considered and using the mean-field approximation introduces a new energy contribution for the field split triplet states given by $\varepsilon_{\text{exch}}=2J\langle\mu\rangle zm_s$ where J is the exchange coupling, z the coordination number, and $m_s=0,\pm1$ is the spin quantum number. Introduction of the AFM correlation energy leads to the following expression for the magnetization per spin $M/Ng\mu_B$:

$$\frac{\langle\mu\rangle}{g\mu_B}=\frac{2\sinh[g\mu_B\mu_0H/k_BT+2Jz\langle\mu\rangle/k_BT]}{\exp[(\Delta+D)/T]+\exp(D/T)+2\cosh[g\mu_B\mu_0H/k_BT+2Jz\langle\mu\rangle/k_BT]}. \tag{3}$$

Equation (3) is solved for $\langle\mu\rangle/g\mu_B$ self-consistently using a graphical method.

We note that alternative approaches have been used to fit the susceptibility behavior. Raedelli and Cheong[25] base their qualitative treatment on a three-state (LS, IS, and HS) model which they link to their high-resolution neutron-diffraction findings on bond length changes with temperature. Kyômen *et al.*[11,13] have fitted the susceptibility and specific heat data for LCO using a phenomenological molecular-field model that allows for an entropy of mixing of Co ions in different spin states. Various possible arrangements of the LS and HS ions are proposed. The present model with explicit allowance for AFM couplings involves few assumptions. In particular no constraints are placed on the spin configurations and spin dynamics. Further work is needed to determine whether changes in properties of LCO, including the susceptibility, at temperatures above 200 K can be explained using the present approach with inclusion of the higher energy levels.

V. COMPARISON WITH EXPERIMENT

The plotted points in Fig. 6 show the experimental $\langle\mu\rangle/g\mu_B$ versus T results derived from the magnetization measurements. We find that Eq. (3) with $J=0$ plus the g value and Δ from EPR, predicts $\langle\mu\rangle/g\mu_B$ values that are much too large and do not match the data. This can be seen in the inset in Fig. 6. Allowance for AFM interactions be-

tween Co ions in the triplet state permits the fit to the experimental $\langle\mu\rangle/g\mu_B$ values shown in Fig. 6 with the theoretical curve based on the solution of Eq. (3) using $g=3.4$, $z=6$, and the following values for the other fitting parameters: $\Delta=150$ K, $D=7$ K, and $2J=-55$ K. Agreement between the model and experiment is generally very good except at low T where paramagnetic impurities produce an upturn in the magnetization and at temperatures well above the maximum where the experimental values decrease more rapidly than the model predicts. We emphasize that the simple singlet-triplet model ignores the higher states shown in Fig. 1(a) and the predictions are expected to be unreliable for $T>200$ K. The good fit to the magnetization data obtained for $T<200$ K provides strong support for the AFM model. Furthermore, the value obtained for Δ is in fair agreement with the rough estimate based on the EPR signal intensity versus T plot[16] and the g value is consistent with the previous EPR results.[16] The curve in Fig. 6 is insensitive to changes in the small value of D but depends sensitively on J and Δ in a two parameter fit if g is kept fixed. The value for D is close to the value obtained in neutron-scattering experiments.[23]

Using the model based on the energy states depicted in Fig. 1(b), with the parameters derived from the $\langle\mu\rangle/g\mu_B$ versus T fit procedure described above, the spin contribution to the molar specific heat C can be estimated. From the partition function we obtain, to a good approximation, the spin contribution to C for $H=0$ as

$$C_{\text{spin}} = 3R\left(\frac{\Delta}{T}\right)^2 \frac{(1+6e^{-\Delta/T})}{(6+e^{\Delta/T}+9e^{-\Delta/T})}. \tag{4}$$

A similar expression applies for magnetic fields that are not too large (<10 T). The Zeeman and AFM terms can be neglected at the temperatures of interest ($T<100$ K), where the spin contribution to the specific heat is significant, as a consequence of the comparatively large gap between the nonmagnetic ground state and the excited triplet states. Expanding exponential factors that involve the Zeeman and AFM interactions it can be shown that, these contributions may be neglected.

Together with the measured C values the calculated temperature dependence of the spin contribution to the specific heat, based on Eq. (4), is shown in Fig. 7(a) using $\Delta=150$ K. The measured 0 and 9 T results coincide within experimental uncertainty consistent with the model predictions. Figure 7(a) shows what is called the corrected specific heat (C_{expt}-C_{spin}), obtained by subtracting the theoretical spin contribution from the measured values. It is possible, by introducing a number of parameters, to fit the corrected specific-heat curve using a Debye-Einstein model that allows for acoustic and optic modes as presented in Fig. 7(b). The plotted Debye contribution corresponds to a chosen Debye temperature $\theta_D=300$ K. While there is uncertainty in θ_D and a somewhat higher value may apply, the large departure of the Debye model predictions from the measured specific heat for $T>50$ K points to the importance of optic modes. Using available infrared spectroscopy results for $LaCoO_3$ (Ref. 26) three optic modes have been included using the Einstein approximation with $\theta_D=255$, 453, and 778 K. Together with the Debye contribution the resulting curve gives a reasonable fit to the spin corrected specific heat below 200 K. For the present discussion we are interested in the low-temperature specific heat and the relatively small and field insensitive spin component of the specific heat as predicted by the model is consistent with the observations. Only at much higher magnetic fields where the singlet-triplet gap closing condition is approached, or reached, will the spin contribution to the specific heat become significant.

VI. CONCLUSION

Taken together, EPR, magnetization, and specific heat measurements support a model for the thermally activated Co^{3+} spin state transition in LCO from a low spin singlet state to a triplet excited state corresponding to an effective spin $S_{\text{eff}}=1$ in the manifold of high spin $S=2$ states. Spin-orbit coupling, crystal-field effects, and the small trigonal distortion of the lattice are important in determining the EPR spectra, and the associated spin-Hamiltonian parameters for this system, at temperatures in the range 20–70 K. Extreme broadening of the EPR spectral lines above 70 K, attributed to spin state lifetime effects, prevented measurements at higher temperatures. In fitting the magnetization data using a model based on the low-lying Co^{3+} spin states it is found necessary to allow for AFM couplings between spins in the excited triplet state. Evidence for the importance of AFM effects is provided by the measured magnetic susceptibility above 130 K where Curie-Weiss behavior is found. The parameters obtained from the mean-field model fit to the spin magnetization data have been used to estimate the spin contribution to the specific heat as a function of applied field. Both the measurements and the model calculations show that the spin contribution to the specific heat is of minor importance for applied fields up to 9 T. The results show that the major contribution to spin-dependent physical properties in the present work is due to the thermally induced population of the low-lying triplet state. While the model is not expected to provide a good description of the LCO properties at temperatures well above 200 K, where higher levels in the spin multiplet become increasingly important, it satisfactorily explains the present single-crystal observations in the temperature range 4–200 K.

ACKNOWLEDGMENTS

Financial support under Cooperative Agreement No. DMR–0234125 and by the State of Florida is gratefully acknowledged. Work carried out at Argonne National Laboratory was supported by the U.S. Department of Energy, Office of Science, under Contract No. DE-AC02-06CH11357.

[1] P. M. Raccah and J. B. Goodenough, Phys. Rev. **155**, 932 (1967).
[2] M. A. Señarís-Rodríguez and J. B. Goodenough, J. Solid State Chem. **116**, 224 (1995).
[3] M. Abbate, J. C. Fuggle, A. Fujimori, L. H. Tjeng, C. T. Chen, R. Potze, G. A. Sawatzky, H. Eisaki, and S. Uchida, Phys. Rev. B **47**, 16124 (1993).
[4] K. Asai, O. Yokokura, N. Nishimori, H. Chou, J. M. Tranquada, G. Shirane, S. Higuchi, Y. Okajima, and K. Kohn, Phys. Rev. B **50**, 3025 (1994).
[5] M. Itoh and I. Natori, J. Magn. Magn. Mater. **140-144**, 2145 (1995).
[6] S. Yamaguchi, Y. Okimoto, H. Taniguchi, and Y. Tokura, Phys. Rev. B **53**, R2926 (1996).
[7] M. A. Korotin, S. Yu. Ezhov, I. V. Solovyev, V. I. Anisimov, D. I. Khomskii, and G. A. Sawatzky, Phys. Rev. B **54**, 5309 (1996).
[8] T. Saitoh, T. Mizokawa, A. Fujimori, M. Abbate, Y. Takeda, and M. Takano, Phys. Rev. B **55**, 4257 (1997).
[9] Y. Kobayashi, N. Fujiwara, S. Murata, K. Asai, and H. Yasuoka, Phys. Rev. B **62**, 410 (2000).
[10] C. Zobel, M. Kriener, D. Bruns, J. Baier, M. Grüninger, T. Lorenz, P. Reutler, and A. Revcolevschi, Phys. Rev. B **66**, 020402(R) (2002).
[11] T. Kyômen, Y. Asaka, and M. Itoh, Phys. Rev. B **67**, 144424 (2003).
[12] D. I. Khomskii and U. Löw, Phys. Rev. B **69**, 184401 (2004).
[13] T. Kyômen, Y. Asaka, and M. Itoh, Phys. Rev. B **71**, 024418 (2005).
[14] M. W. Haverkort, Z. Hu, J. C. Cezar, T. Burnus, H. Hartmann, M. Reuther, C. Zobel, T. Lorenz, A. Tanaka, N. B. Brookes, H. H. Hsieh, H.-J. Lin, C. T. Chen, and L. H. Tjeng, Phys. Rev. Lett. **97**, 176405 (2006).
[15] R. F. Klie, J. C. Zheng, Y. Zhu, M. Varela, J. Wu, and C. Leighton, Phys. Rev. Lett. **99**, 047203 (2007).
[16] S. Noguchi, S. Kawamata, K. Okuda, H. Nojiri, and M. Motokawa, Phys. Rev. B **66**, 094404 (2002).
[17] Z. Ropka and R. J. Radwanski, Phys. Rev. B **67**, 172401 (2003).
[18] T. L. Phan, L. V. Bau, N. V. Khiem, N. X. Phuc, and S. C. Yu, Phys. Status Solidi B **242**, 1522 (2005).
[19] D. P. Kozlenko, N. O. Golosova, Z. Jirák, L. S. Dubrovinsky, B. N. Savenko, M. G. Tucker, Y. Le Godec, and V. P. Glazkov, Phys. Rev. B **75**, 064422 (2007).
[20] J. van Tol, L.-C. Brunel, and R. J. Wylde, Rev. Sci. Instrum. **76**, 074101 (2005).
[21] A. K. Hassan, L. A. Pardi, J. Krystek, A. Sienkiewicz, P. Goy, M. Rohrer, and L.-C. Brunel, J. Magn. Reson. **142**, 300 (2000).
[22] A. Abragam and B. I. Bleaney, *Electron Paramagnetic Resonance of Transition Ions* (Clarendon, Oxford, 1970).
[23] D. Phelan, Despina Louca, S. Rosenkranz, S.-H. Lee, Y. Qiu, P. J. Chupas, R. Osborn, H. Zheng, J. F. Mitchell, J. R. D. Copley, J. L. Sarrao, and Y. Moritomo, Phys. Rev. Lett. **96**, 027201 (2006).
[24] J. Wu and C. Leighton, Phys. Rev. B **67**, 174408 (2003).
[25] P. G. Radaelli and S.-W. Cheong, Phys. Rev. B **66**, 094408 (2002).
[26] S. Yamaguchi, Y. Okimoto, and Y. Tokura, Phys. Rev. B **55**, R8666 (1997).